European Journal of Nuclear Medicine and Molecular Imaging (2020) 47:1412–1426
https://doi.org/10.1007/s00259-019-04607-x

ORIGINAL ARTICLE

Targeting MMP-14 for dual PET and fluorescence imaging of glioma in preclinical models

Benjamin B. Kasten[1] · Ke Jiang[2] · Denzel Cole[3] · Aditi Jani[4] · Neha Udayakumar[4] · G. Yancey Gillespie[1] · Guolan Lu[5] · Tingting Dai[2] · Eben L. Rosenthal[5] · James M. Markert[1] · Jianghong Rao[2] · Jason M. Warram[3]

Received: 14 August 2019 / Accepted: 7 November 2019 / Published online: 26 November 2019

Abstract

Purpose There is a clinical need for agents that target glioma cells for non-invasive and intraoperative imaging to guide therapeutic intervention and improve the prognosis of glioma. Matrix metalloproteinase (MMP)-14 is overexpressed in glioma with negligible expression in normal brain, presenting MMP-14 as an attractive biomarker for imaging glioma. In this study, we designed a peptide probe containing a near-infrared fluorescence (NIRF) dye/quencher pair, a positron emission tomography (PET) radionuclide, and a moiety with high affinity to MMP-14. This novel substrate-binding peptide allows dual modality imaging of glioma only after cleavage by MMP-14 to activate the quenched NIRF signal, enhancing probe specificity and imaging contrast.

Methods MMP-14 expression and activity in human glioma tissues and cells were measured in vitro by immunofluorescence and gel zymography. Cleavage of the novel substrate and substrate-binding peptides by glioma cells in vitro and glioma xenograft tumors in vivo was determined by NIRF imaging. Biodistribution of the radiolabeled MMP-14-binding peptide or substrate-binding peptide was determined in mice bearing orthotopic patient-derived xenograft (PDX) glioma tumors by PET imaging.

Results Glioma cells with MMP-14 activity showed activation and retention of NIRF signal from the cleaved peptides. Resected mouse brains with PDX glioma tumors showed tumor-to-background NIRF ratios of 7.6–11.1 at 4 h after *i.v.* injection of the peptides. PET/CT images showed localization of activity in orthotopic PDX tumors after *i.v.* injection of ^{68}Ga-binding peptide or ^{64}Cu-substrate-binding peptide; uptake of the radiolabeled peptides in tumors was significantly reduced ($p < 0.05$) by blocking with the non-labeled-binding peptide. PET and NIRF signals correlated linearly in the orthotopic PDX tumors. Immunohistochemistry showed co-localization of MMP-14 expression and NIRF signal in the resected tumors.

Conclusions The novel MMP-14 substrate-binding peptide enabled PET/NIRF imaging of glioma models in mice, warranting future image-guided resection studies with the probe in preclinical glioma models.

Keywords MMP-14 · Glioma · NIRF · PET · Molecular imaging · Dual modality

Benjamin B. Kasten and Ke Jiang contributed equally to this work.

This article is part of the Topical Collection on Preclinical Imaging

Electronic supplementary material The online version of this article (https://doi.org/10.1007/s00259-019-04607-x) contains supplementary material, which is available to authorized users.

✉ Jianghong Rao
jrao@stanford.edu

✉ Jason M. Warram
mojack@uab.edu

[1] Department of Neurosurgery, University of Alabama at Birmingham, Birmingham, AL 35294, USA

[2] Departments of Radiology and Chemistry, Molecular Imaging Program at Stanford, Stanford University School of Medicine, Stanford, CA 94305, USA

[3] Department of Otolaryngology, University of Alabama at Birmingham, Birmingham, AL 35294, USA

[4] School of Medicine, University of Alabama at Birmingham, Birmingham, AL 35294, USA

[5] Department of Otolaryngology – Head and Neck Surgery, Stanford University, Stanford, CA 94305, USA

Introduction

Malignant glioma is the most common and deadly primary brain malignancy in adults. The current standard of care, comprised of maximal safe surgical resection followed by radiochemotherapy, is associated with a median survival of less than 18 months [1]. Clinical trials are testing novel therapeutic strategies in attempts to improve the current prognosis of patients with glioma. Studies have shown that the extent of surgical resection correlates with patient outcomes [2, 3]. Unfortunately, malignant tissues are frequently difficult to differentiate from normal brain parenchyma, making complete surgical resection of all glioma while sparing vital healthy brain a significant clinical challenge. Developing agents that specifically target aggressive glioma cells for both non-invasive and intraoperative imaging is an attractive strategy to guide effective therapeutic intervention. Glioma is known for its invasive and diffuse growth pattern, which is indicative of matrix metalloproteinase (MMP) activity [4–7]. Activated MMP-14, also called MT1-MMP, is overexpressed in glioma while it is not expressed at significant levels in normal brain (cerebral) tissue. MMP-14 expression is known to increase with the grade of glioma and correlates with poor patient outcome [8–11]. Preclinical studies have demonstrated that MMP-14 can be exploited as a biomarker for molecular imaging of glioma with various non-invasive or intraoperative reporting modalities [12–14].

Non-invasive imaging of glioma patients through positron emission tomography (PET) with radiolabeled amino acid analogs has enabled preoperative planning for biopsy or surgery, mapping for radiotherapy, and assessing therapeutic response [15–22]. However, clinical PET suffers from low spatial resolution (> 3 mm) and does not permit real-time surgical guidance. Problems with brain shift further hamper co-registration of PET and anatomical images. While clinical PET complements the information from MRI [23], these modalities remain insufficient to guide real-time surgical resection of occult glioma. The US Food and Drug Administration (FDA) recently approved 5-aminolevulinic acid (5-ALA), which is converted into the fluorescent metabolite protoporphyrin IX (PpIX) in rapidly proliferating tumor cells (e.g., glioma), for fluorescence-guided surgical resection of glioma. Phase III trials have shown 5-ALA fluorescence-guided resection in glioma patients was well tolerated and mediated greater rates of complete resection compared to MRI alone [24, 25]. Nonetheless, the optical properties of PpIX are not ideal for in vivo imaging. Significant tissue autofluorescence and photon attenuation at the wavelengths of excitation (~ 405 nm) and emission (635 nm) reduce spatial resolution and tumor-to-background ratios (TBRs) associated with 5-ALA imaging of glioma [26–28]. Molecular imaging strategies that use near-infrared fluorescence (NIRF) reporters are attractive for in vivo imaging and fluorescence-guided resection due to the minimal tissue autofluorescence and significantly less photon attenuation in the NIR window (700–900 nm) [29–31]. Several molecular targeted compounds with NIRF reporters are currently being evaluated for resecting glioma in preclinical and clinical studies [14, 29, 30, 32–34].

The purpose of the present work was to design a novel, MMP-14-activatable dual PET/NIRF peptide probe for imaging and guiding resection of glioma (Fig. 1). The peptide probe combined (1) a NIRF reporter and quencher pair separated by a peptide sequence (MMP-14 "substrate peptide") that is cleaved specifically by activated MMP-14 to release the quencher and allow visualization of the NIRF dye and (2) a chelate for radionuclides attached to a peptide sequence that binds to MMP-14 (MMP-14 "binding peptide") and enables PET imaging. The following in vitro and in vivo studies tested the ability of these MMP-14-targeted imaging probes to detect preclinical models of human glioma. Glioma cells in vitro and orthotopic xenograft tumors in mice in vivo cleaved the substrate and the substrate-binding peptides to activate the NIRF signal of the initially quenched peptide probes, yielding favorable imaging contrast in tumors relative to the normal brain. In vivo PET/CT imaging showed notable activity in orthotopic glioma tumors relative to normal brain after *i.v.* injection of the radiolabeled-binding or substrate-binding peptides. PET and NIRF signals from the substrate-binding peptide correlated linearly in the orthotopic PDX tumors and co-localized with MMP-14 expression in the resected tumors. The results from these initial studies indicate the success of the proposed dual-modality imaging strategy to detect MMP-14 in glioma models with the first-generation substrate-binding peptide probe.

Results

Human glioma tumor tissues and cell lines express varying levels of MMP-14

Immunofluorescence staining of a human glioma tissue microarray was performed to determine the relative protein expression of MMP-14 in glioma and normal brain specimens. Consistent with previous reports [8–11], the immunofluorescence results showed significant overexpression of MMP-14 in all grades of glioma relative to normal cerebral tissue (1.6 ± 0.6, 2.2 ± 0.7, 2.5 ± 0.8, 3.0 ± 1.2 glioma/normal brain ratios for grade 1, grade 2, grade 3, and grade 4, respectively; $p < 0.05$), with highest expression in grade 4 glioma (Fig. 2A). Western blot, immunofluorescence, and gel zymography studies were then performed to characterize the in vitro expression and activity of MMP-14 and MMP-2 in immortalized human glioma cell lines. Absolute expression of MMP-14 does not necessarily correlate to MMP-14 activity, as the latter is regulated partly through tissue inhibitors of metalloproteinases (TIMPs). For instance, TIMP-2 binds to the catalytic domain

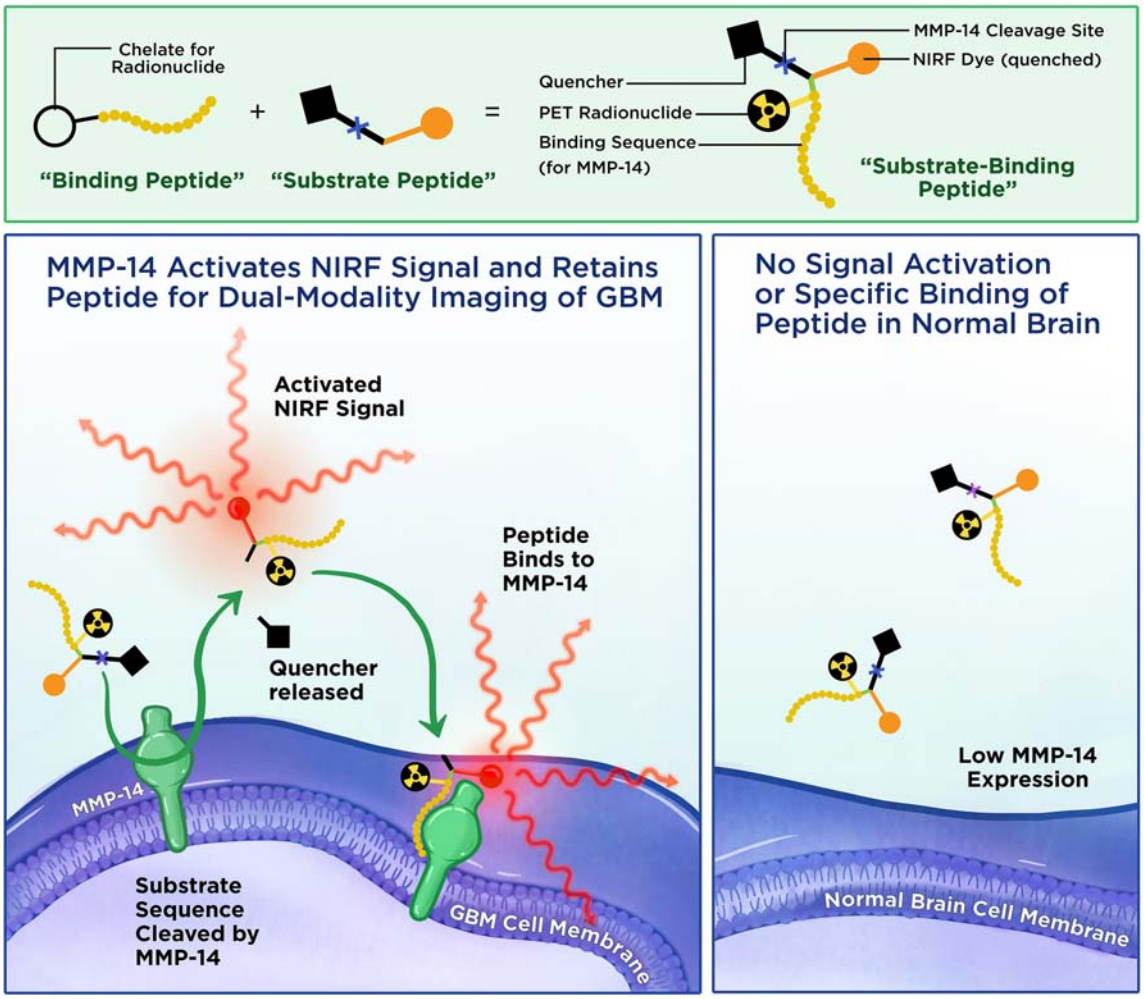

Fig. 1 Diagram showing general scheme for dual-modality PET/NIRF imaging of glioma (GBM) with an MMP-14 activatable peptide

of MMP-14, thus blocking enzymatic activity. TIMP-2 is also required in a ternary complex with MMP-14 and proMMP-2 prior to enzymatic cleavage by a second MMP-14 enzyme to activate MMP-2 [7]. U251 cells in our studies displayed the highest expression of MMP-14 by immunofluorescence (Fig. 2B) and Western blot analyses (Fig. S1A,B), while U87 cells displayed the highest level of MMP-14 activity as indirectly determined through gel zymography analyses of MMP-2 activity (Fig. 2C), which is catalyzed by MMP-14 as described [5, 35]. U87 cells showed the highest MMP-2 expression by Western blot (Fig. S1C,D). Although TIMP expression was not determined in our studies, the zymography assay confirmed MMP-14 activity in the glioma cells. These results indicate the cell lines would be suitable in assays that employ peptide probes as enzymatic substrates for MMP-14.

Description of the novel MMP-14 activatable peptide probes

We and others have used an MMP-14 substrate peptide sequence (RSCitG-HPhe-YLY) to generate peptide probes for imaging and therapy studies in human xenograft tumors that over-express MMP-14 [36–38]. For the present studies, this sequence was used between the NIRF IRDye800 and quencher IR QC-1 pair [39, 40] to generate the MMP-14 activatable NIRF substrate peptide (Supplementary Fig. S2). This strategy allows the initially quenched signal from IRDye800, which is suitable for NIRF imaging in vivo, to become activated upon cleavage of the peptide by MMP-14. For the second peptide component, an MMP-14-binding peptide sequence (HWKHLHNTKTFL) was selected that has previously been described with an apparent k_d of 47.4 nM for MMP-14 [41]. This binding peptide sequence has been joined to various reporting moieties and used in a rat orthotopic glioma model [12] as well as human xenograft tumors that overexpress MMP-14 [41–43]. For the present studies, a derivative of the NOTA (1,4,7-triazacyclononane-1,4,7-triacetic acid) chelate for coordination with ^{64}Cu(II) or ^{68}Ga(III) was attached to the peptide sequence to generate the MMP-14-binding peptide (Supplementary Fig. S3) for in vivo PET imaging of MMP-14 expression. The two peptide precursors were synthesized separately by standard solid phase synthesis, NHS, and

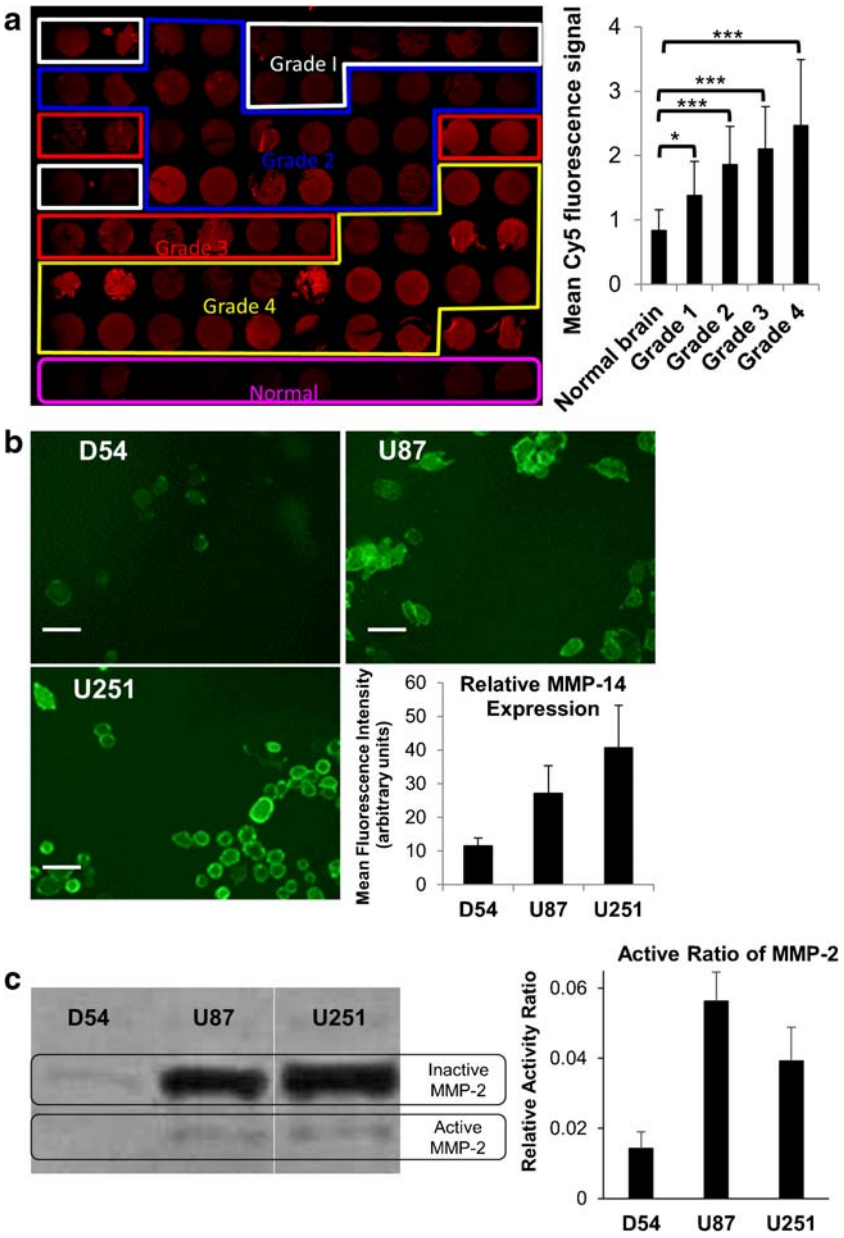

Fig. 2 Human glioma patient specimens and cell lines grown in vitro express different levels of MMP-14. **A** MMP-14 immunofluorescence (left) and quantification of fluorescence signal (right) in a human tissue microarray (mean ± SD, n = 10–24 tissue sections/group); **B** MMP-14 immunofluorescence of adherent GBM cells grown in vitro and quantification of fluorescence signal (bottom right; mean ± SD, n = 25–30/group); **C** MMP-2 gel zymography (left) and quantification of relative active/latent MMP-2 band intensity (right) from supernatants of adherent GBM cells grown in vitro (mean ± SD, n = 3/group); scale bar in B, 20 μm; *$p < 0.05$; ***$p < 0.001$

maleimide coupling reactions and then joined via a cycloaddition reaction between the azide and alkyne moieties present on the corresponding precursor peptides to generate the combined MMP-14 substrate-binding peptide (Supplementary Fig. S4). Mass spectroscopic analyses were consistent with the anticipated peptide structures (Supplementary Figs. S5, S6, S7).

MMP-14 and human glioma cells activate the NIRF signals of the MMP-14 peptide probes in vitro

With the novel MMP-14-targeted peptides in hand, in vitro NIRF activation studies with the catalytic domain of MMP-14 were performed. Previous studies have shown that appending fluorescence dyes or other moieties to the N- and C-termini of the core substrate peptide sequence does not abrogate cleavage of the peptide by MMP-14 [37, 44]. However, studies to date have not determined if incorporation of an MMP-14-binding ligand into the same scaffold as an MMP-14 substrate sequence affects cleavage of the substrate peptide by the enzyme.

As presented in Fig. 3A, both the substrate and the substrate-binding peptides showed NIRF activation over time relative to the quenched starting moieties during incubation with MMP-14. The relative NIRF activation of the substrate peptide appeared to stabilize within the first 10 min, while NIRF activation of the substrate-binding peptide continued to increase beyond 1 h. The fold of increase in the

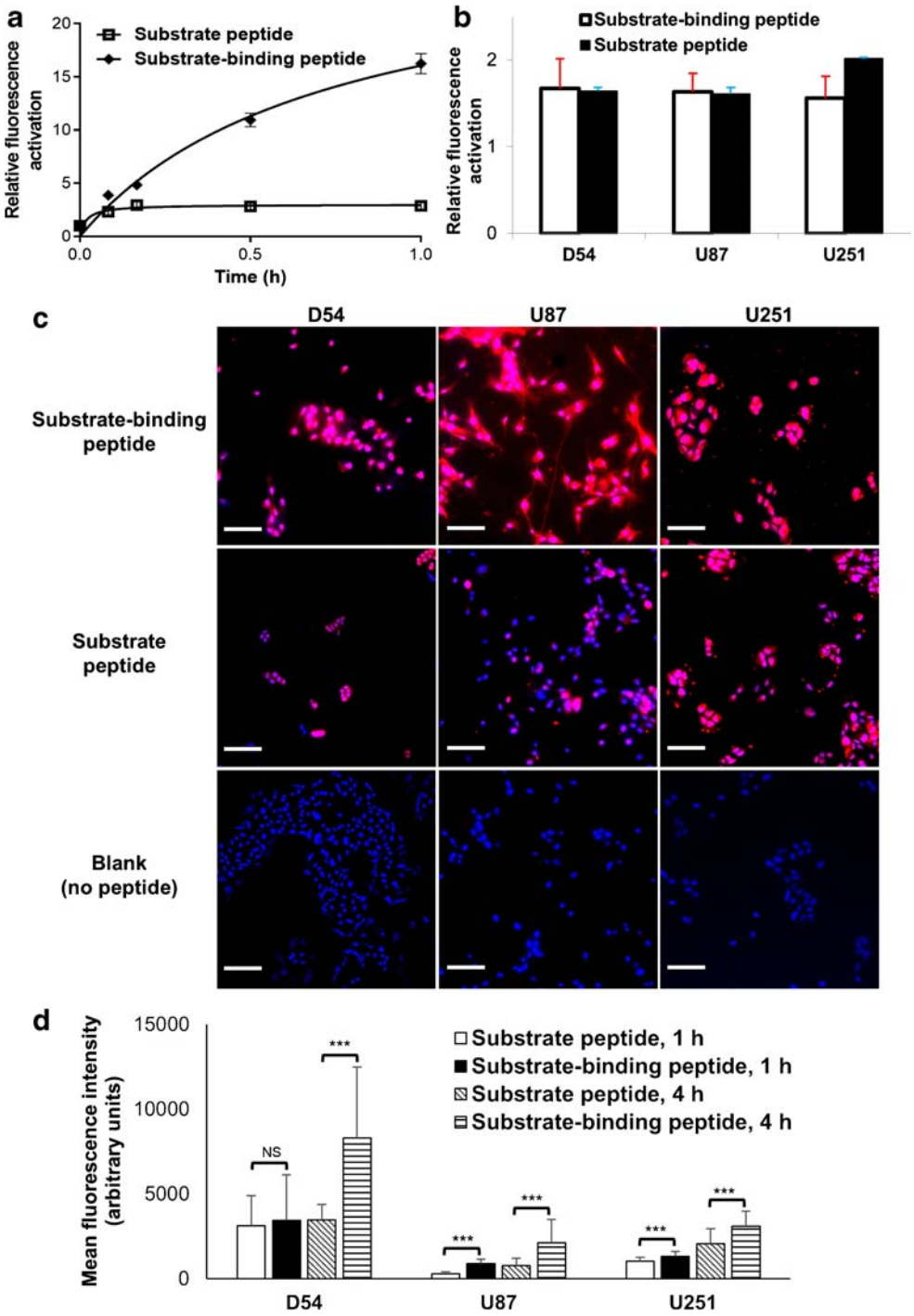

Fig. 3 Human MMP-14 enzyme and glioma cells activate the NIRF signals of the MMP-14 peptides in vitro. **A**, relative increase in NIRF activation at various time points (0–1 h) after incubating the substrate-binding peptide or the substrate peptide (0.5 μM) with the recombinant catalytic domain of MMP-14 at 37 °C. **B**, relative increase in NIRF activation released into the supernatant after incubating the substrate-binding peptide or the substrate peptide (0.5 μM) with human glioma cell lines (D54, U87, U251) at 37 °C for 2 h (mean ± SD, n = 2–4/group). **C**, NIRF microscopy showing the cell-associated NIRF signal (red) in glioma cells (D54, U87, U251) 1 h after incubation with the substrate-binding peptide (top), substrate peptide (middle), or buffer control without peptide (bottom); cell nuclei were counter-stained with DAPI (blue); scale bar: 50 μm. **D**, quantification of cell-associated NIRF signal at 1 or 4 h after incubating glioma cells in vitro with the substrate or substrate-binding peptide (mean ± SD, n = 30/group). ***$p < 0.001$; NS, not significant

fluorescence with the substrate-binding peptide was much higher than that with the substrate peptide. Based on these initial results, it is possible that the binding sequence may influence the kinetics of the substrate-binding peptide cleavage reaction by MMP-14.

NIRF signal activation of the substrate and substrate-binding peptides was apparent in supernatant solutions (Fig. 3B) and associated with the cells (Fig. 3C) during in vitro incubation with the glioma cell lines. Similar increases in NIRF intensities released into the supernatant were observed during incubation of the peptides with all three glioma cell lines (Fig. 3B) regardless of their relative expression of active MMP-14 (Fig. 2C). NIRF microscopy showed that U87 and U251 cells had significantly higher cell-associated mean NIRF signal at both 1 and 4 h after incubation with the substrate-binding peptide relative to the substrate peptide ($p < 0.001$) at the respective time points (Fig. 3D). In D54 cells, which had lower MMP-14 expression and activity relative to

the other cells (Fig. 2B,C), the cell-associated NIRF signal was significantly higher for the substrate-binding peptide compared to the substrate peptide at 4 h ($p < 0.001$) but not at 1 h ($p > 0.05$; Fig. 3D). These results are consistent with the anticipated mechanism of the substrate-binding peptide, where the MMP-14 binding moiety mediates cellular retention of the residual fluorophore-containing product following cleavage of the substrate sequence by MMP-14. The observed NIRF signal associated with cells incubated with the substrate peptide, which lacks the MMP-14-binding component, likely indicates nonspecific cell uptake of the substrate peptide or the fluorophore-containing product following cleavage by MMP-14. Collectively, these results indicate that glioma cells, including those with relatively low MMP-14 activity, are capable of cleaving the novel peptide substrates in vitro.

NIRF signals of the MMP-14 activatable peptide probes localize in human glioma xenografts in nude mice in vivo

Having confirmed that glioma cells activate the NIRF signal of the peptides in vitro, NIRF imaging studies were performed to determine if the peptide probes showed uptake in glioma xenograft tumors in vivo. At 24 h after *i.v.* injection of the substrate-binding peptide, in vivo NIRF imaging showed a low TBR (1.3 ± 0.2 relative to muscle) in subcutaneous (*s.c.*) D54 tumors and significantly higher TBR in *s.c.* U87 tumors (2.2 ± 0.4; $p < 0.001$) (Fig. 4A, B). Low NIRF signal was observed in all normal tissues except the kidneys (Fig. 4A), indicating predominantly renal clearance of the peptide. *S.c.* U87 tumors from groups of mice injected *i.v.* with either the substrate peptide or the substrate-binding peptide showed no significant difference in TBR or mean NIRF intensity at the 24 h time point (Supplementary Fig. S8). These initial studies demonstrated that glioma tumors show uptake of NIRF signal after administering the quenched peptide substrates. The moderate NIRF TBRs observed for the flank tumors could be due to endogenous expression of MMP-14 in the tissues surrounding the tumors (e.g., muscle, skin) [45].

NIRF imaging studies with the substrate or substrate-binding peptides were subsequently performed in mice bearing orthotopic patient-derived xenograft (PDX) glioma tumors. Relative to flank xenografts of immortalized cell lines, these orthotopic PDX tumors more accurately retain characteristics of clinical glioma [46, 47]. Furthermore, orthotopic tumors were anticipated to better demonstrate the signal contrast from the peptide probes in glioma tumors relative to the endogenous surrounding tissue (e.g., normal brain). The low expression of MMP-14 in normal brain was anticipated to result in a low background NIRF signal, resulting in a higher and more appropriate TBR in the orthotopic glioma tumor model than was observed in

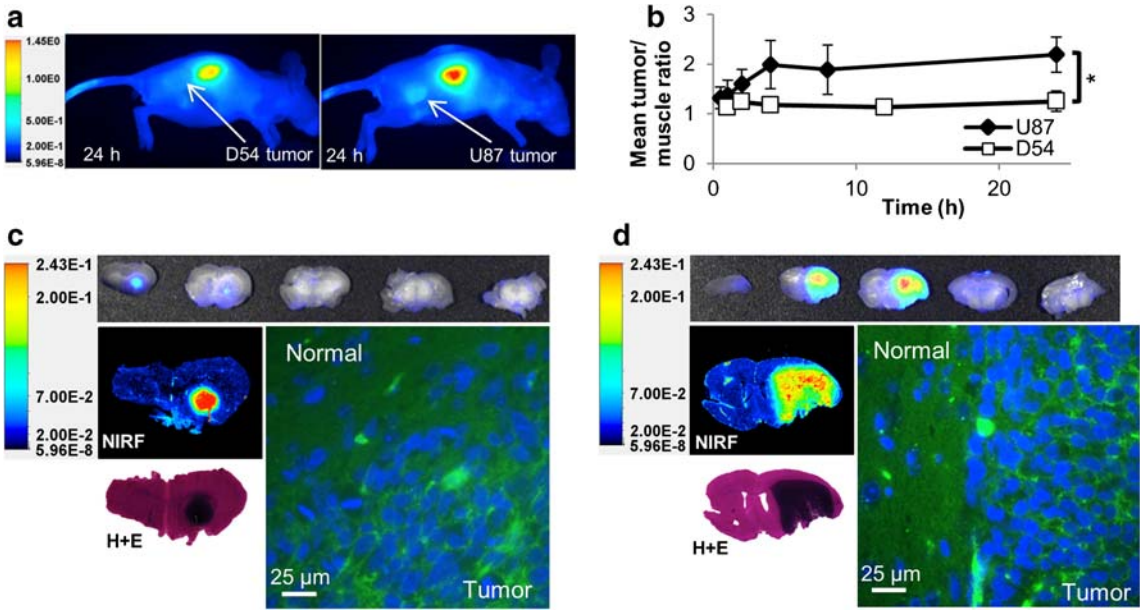

Fig. 4 NIRF signals from the MMP-14 peptide probes localize in human glioma xenograft tumors in mice in vivo. **A**, in vivo NIRF images of live mice bearing flank D54 or U87 glioma tumors at 24 h after *i.v.* injection of the substrate-binding peptide. **B**, mean in vivo tumor/muscle NIRF ratios at various time points (0.25–24 h) after injection of the substrate-binding peptide in mice bearing flank D54 or U87 glioma tumors (mean ± SD, n = 5 mice/group). **C**,**D**, mice bearing orthotopic PDX JX12 glioma tumors were injected *i.v.* either with the substrate peptide (C) or with the substrate-binding peptide (D). Mice were euthanized 1 h later, when the brains were resected, fixed in formalin overnight and serially sectioned (2 mm). Gross tissue NIRF imaging (Pearl system) showed localization of NIRF signals in the serial tumor-bearing sections (2 mm sections, top panels), as confirmed by higher resolution NIRF imaging (Odyssey system) of 5 μm tissue sections and H + E stained 5 μm tissue sections. NIRF microscopy of DAPI-stained tissue sections (5 μm, right panels, 630× magnification) showed NIRF signal accumulation (yellow channel) in the leading tumor edge but not adjacent normal brain (blue channel, DAPI). *$p < 0.05$

the flank tumor studies. High contrast of the NIRF signal in PDX JX12 tumors relative to adjacent normal brain was apparent in gross slices of resected brains at 1, 4, and 24 h after *i.v.* injection of either the substrate peptide (Fig. 4C) or the substrate-binding peptide (Fig. 4D). NIRF analyses of gross brain slices from the 4 and 24 h time points (Table 1) showed significantly higher ($p < 0.001$) mean NIRF signal in the tumor relative to adjacent normal brain from mice given the substrate-binding peptide. This result is consistent with retention of the cleaved peptide moiety containing the fluorophore within the tumor and low accumulation of the cleaved peptide in normal brain, which has negligible expression of MMP-14. The NIRF signal in the tumor was significantly higher than in normal brain of mice at 4 h ($p < 0.001$), but not at 24 h ($p = 0.074$), after injection of the substrate peptide. The group of mice analyzed at 24 h after injecting the substrate peptide had fewer evaluable tumors compared to the other groups, which could have impacted the statistical outcome of the NIRF signal comparison in these mice. While the NIRF mean tumor signals and TBRs were higher in mice given the substrate-binding peptide relative to the substrate peptide (Table 1), the TBRs were not significantly different at the time points examined ($p > 0.05$, ANOVA). NIRF microscopy showed dispersion of the activated NIRF signal from the peptides throughout the tumors, including near the leading edge of tumor progression (Figs. 4C, D). Both peptides also yielded positive NIRF signals in regions of diffuse glioma cell growth beyond the bulk tumor (data not shown). Comparing histological tissue sections with confirmed glioma growth by H + E to NIRF signals measured in tissue sections yielded sensitivities above 83% for the substrate peptide and above 85% for the substrate-binding peptide (Supplementary Table S1) at the 4 h and 24 h time points. These results confirmed that the novel MMP-14 peptides could be used for NIRF imaging of orthotopic models of human glioma. These findings support future studies that utilize the peptides for intraoperative resection of preclinical glioma tumors in vivo.

PET signals of the radiolabeled MMP-14 peptide probes localize in human glioma orthotopic xenografts in nude mice in vivo

The second goal of this work was to determine if the peptides could be used for in vivo PET imaging of orthotopic models of human glioma tumors in mice. A preliminary study was performed using the binding peptide labeled with ^{68}Ga (^{68}Ga-binding peptide) in mice with orthotopic PDX JX12 tumors. The radiolabeled peptide was obtained in 87–91% radiochemical conversion after heating with ^{68}Ga at 90 °C for 20 min; further heating did not improve the yield of the product ^{68}Ga-binding peptide (Supplementary Fig. S9). Tumor-bearing mice were dosed *i.v.* with 0.4–0.8 nmol ^{68}Ga-binding peptide from the diluted reaction solution (molar activity approximately 6.1 GBq/μmol at time of dosing). At 2 h after dosing, the tumors were visible during PET/CT imaging, while normal brain showed low uptake of activity (Fig. 5A). Ex vivo biodistribution analyses indicated significantly more uptake of radioactivity in brains of mice injected with ^{68}Ga-binding peptide (0.16 ± 0.02 %ID/g) compared to brains of mice injected with ^{68}Ga-binding peptide and 60-fold excess non-labeled-binding peptide as a blocking agent (0.07 ± 0.02 %ID/g, $p < 0.01$) (Fig. 5B), thus supporting the specific retention of the radiolabeled peptide in the PDX tumors. The amount of ^{68}Ga in resected brains correlated with qualitative tumor burden determined by H + E tissue analyses (Supplementary Fig. S10). PET images and ex vivo biodistribution analyses showed high accumulation of activity in the liver, spleen, and kidneys (Supplementary Figs. S11, S12), which was likely due to the relative hydrophobicity of the peptide at physiological pH.

A separate cohort of mice bearing orthotopic PDX JX12 tumors were used for PET imaging and biodistribution analyses with ^{64}Cu-labeled substrate-binding peptide (^{64}Cu-substrate-binding peptide). ^{64}Cu (12.7 h half-life) was used as the radionuclide with the substrate-binding peptide to allow PET imaging analyses at later time points (e.g., 4 h) that were used in the NIRF imaging studies. The relatively short half-

Table 1 Ex vivo NIRF signal intensities and TBRs from the substrate peptide or the substrate-binding peptide measured in 2 mm gross brain slices from mice bearing orthotopic PDX glioma tumors

	Mean NIRF signal in tumor	Mean NIRF signal in normal brain	*p* value (tumor vs. normal brain NIRF signal)	Mean ± SD TBR (range)
Substrate peptide, 4 h	0.012 ± 0.007	0.002 ± 0.001	< 0.001	7.6 ± 2.9 (2.7–10.9)
Substrate peptide, 24 h	0.011 ± 0.010	0.001 ± 0.00	0.074	8.7 ± 6.3 (2.9–17.1)
Substrate-binding peptide, 4 h	0.024 ± 0.011	0.002 ± 0.001	< 0.001	11.1 ± 4.5 (7.8–18.9)
Substrate-binding peptide, 24 h	0.021 ± 0.010	0.002 ± 0.001	< 0.001	13.3 ± 3.7 (6.0–17.6)

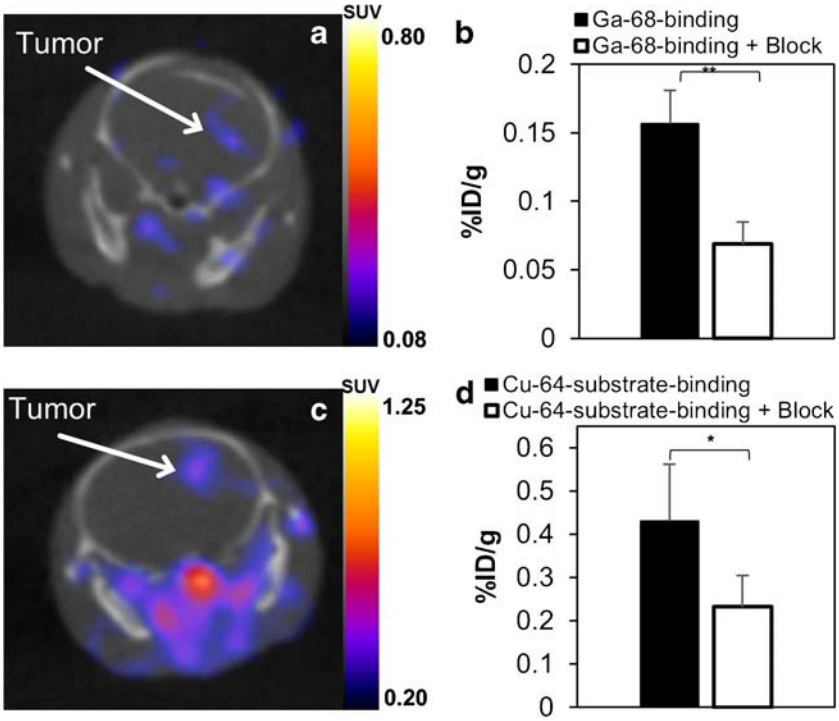

Fig. 5 PET imaging and biodistribution show specific localization of radiolabeled peptide probes in orthotopic PDX glioma tumors in vivo. **A**, representative transverse PET/CT image at 2 h after *i.v.* injection of ^{68}Ga-binding peptide in athymic nude mice bearing orthotopic PDX JX12 glioma tumors, showing localization of activity in the tumor. **B**, ex vivo biodistribution showing whole-brain activity at 3.5 h after *i.v.* injection of ^{68}Ga-binding peptide or of ^{68}Ga-binding peptide + block (non-labeled-binding peptide) in athymic nude mice bearing orthotopic PDX JX12 glioma tumors. Full biodistribution analyses are available in the Supplementary Data. **C**, representative transverse PET/CT image at 4 h after *i.v.* injection of ^{64}Cu-substrate-binding peptide in athymic nude mice bearing orthotopic PDX JX12 glioma tumors, showing localization of activity in the tumor. Activity in soft tissues of the neck (e.g., blood vessels, muscle, lymph nodes) was apparent at the scaling intensity shown in the PET image. **D**, ex vivo biodistribution showing whole-brain activity at 5.5 h after *i.v.* injection of ^{64}Cu-substrate-binding peptide or ^{64}Cu-substrate-binding peptide + block (non-labeled-binding peptide) in athymic nude mice bearing orthotopic PDX JX12 glioma tumors. Full biodistribution analyses are available in the Supplementary Data. *p < 0.05; **p < 0.01; SUV, standardized uptake value

life of ^{68}Ga (67.7 min) precludes PET imaging analyses beyond 3 h. The ^{64}Cu-substrate-binding peptide was generated quantitatively after labeling with ^{64}Cu at room temperature for 20 min (Supplementary Fig. S13). Tumor-bearing mice were dosed *i.v.* with 0.13 nmol ^{64}Cu-substrate-binding peptide from the diluted reaction solution (molar activity approximately 46.6 GBq/μmol at time of dosing). At 4 h after dosing, PET/CT imaging showed significant contrast in the tumor relative to normal brain (Fig. 5C), yielding a standardized uptake value ratio (SUVR: ratio of tumor SUV_{mean} to normal brain SUV_{mean}) of 3.9 ± 0.5. The SUVR was lower in a group of tumor-bearing mice (2.5 ± 1.3) that had been co-injected with 80-fold excess of the non-labeled binding peptide as a blocking agent, although the difference between the two groups of mice was not significant (p = 0.056). The activity present in whole resected brains from mice in the ^{64}Cu-substrate-binding peptide group (0.43 ± 0.13 %ID/g) was significantly higher than that in the blocked group (0.23 ± 0.07 %ID/g; p < 0.05) (Fig. 5D). This result suggests that the binding peptide is able to partially block binding of the substrate-binding peptide to PDX glioma tumors in vivo. Biodistribution analyses of resected tissues were consistent with the PET images, indicating predominantly hepatobiliary accumulation of activity (Supplementary Figs. S14, S15).

NIRF signals from the ^{64}Cu-substrate-binding peptide correlate with PET signals and co-localize with MMP-14 expression in human glioma orthotopic xenografts

The resected brains from mice injected with the ^{64}Cu-substrate-binding peptide in the above studies were sectioned and used for NIRF analyses. Gross imaging showed high contrast between the NIRF signal in PDX tumor regions compared to contralateral normal brain, yielding a TBR of 7.2 ± 1.3 (p < 0.001). The summed NIRF signal from tumor regions in these tissue sections correlated linearly (R^2 = 0.84, p < 0.0001) with the in vivo PET %ID/cm^3 signal present in the tumor-bearing brain regions (Fig. 6A). Microscopic imaging of hematoxylin and eosin (H + E) stained tissue sections confirmed that the NIRF signal co-localized in the PDX glioma tumors, which showed high expression of MMP-14 relative to normal brain (Fig. 6B-G). These results support the hypothesis that the NIRF signal from the cleavable peptide was

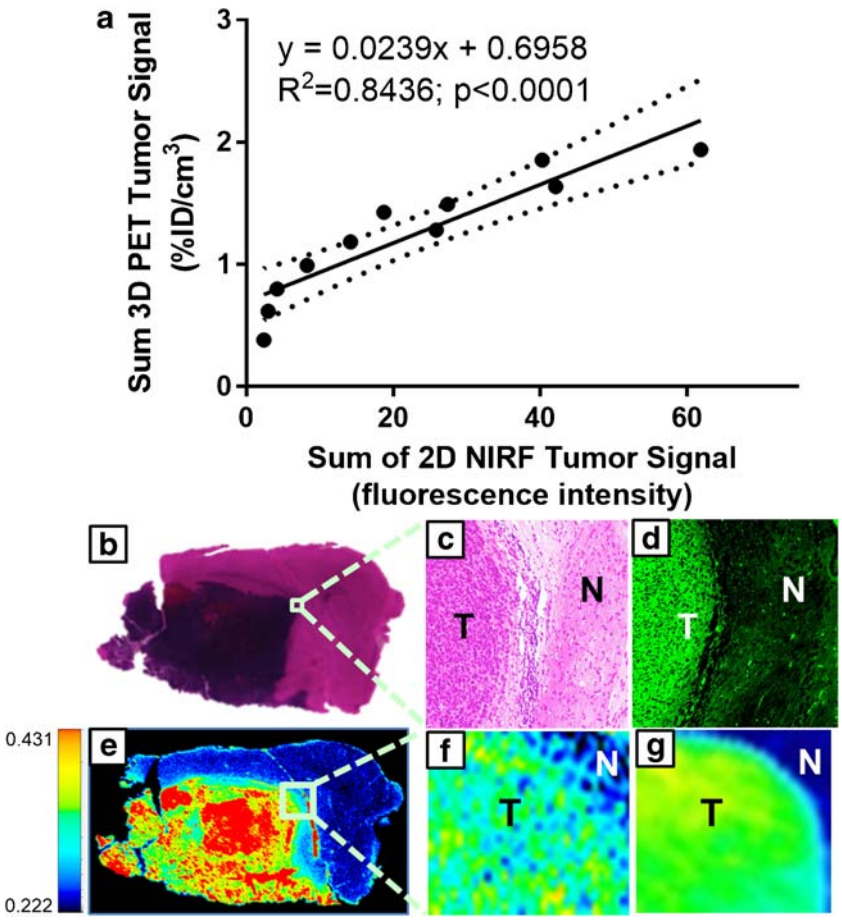

Fig. 6 NIRF signals from the radiolabeled substrate-binding peptide show high concordance with PET signal, orthotopic PDX glioma localization, and MMP-14 expression. **A**, linear correlation between in vivo PET (%ID/cm^3) and ex vivo NIRF signals from brains from mice bearing orthotopic PDX JX12 glioma tumors after *i.v.* injection of the ^{64}Cu-substrate-binding peptide (0.13 nmol); dotted lines show the 95% confidence interval of the correlation. Co-localization of H + E stained tumor (**B**, **C**), IRDye800 fluorescence on Odyssey scanner (**E**, **F**), and MMP-14 expression (**D**, **G**) in brain sections from mice bearing orthotopic PDX JX12 glioma tumors after *i.v.* injection of the ^{64}Cu-substrate-binding peptide. Separate sections were probed using an anti-MMP-14 antibody conjugated to either dye Alexa Fluor 488 for microscopy (**D**) or dye Cy5 for Odyssey scanner (**G**, 21 μm resolution). Microscopic images (**C**, **D**) are 100x. T, tumor; N, normal brain

specifically retained in the PDX glioma tumors due to the expression of MMP-14 in the tumors. The absolute NIRF signal from brains of mice injected with the ^{64}Cu-substrate-binding peptide was lower than that from mice in the study with the non-labeled substrate-binding peptide. This result was anticipated due to the different mass dose of the peptides used for the two studies. These studies support the feasibility of dual-modality PET and NIRF imaging with the radiolabeled peptide probe in a PDX glioma model. A goal of future work will be to determine the effect of the labeled and non-labeled peptide doses on the TBR for the PET and NIRF signals separately.

Discussion

The membrane-bound collagenase MMP-14 is a key enzyme in initiating and propagating the invasive phenotype associated with malignant glioma progression. MMP-14 processes other MMPs (e.g., proMMP-2) to their active state and cleaves adhesion proteins (e.g., CD44, integrins, etc.) in addition to extracellular collagen [5, 35, 48–50]. MMP-14 is also expressed on tumor-associated glial cells and macrophages, which can comprise up to 30% of the tumor bulk and have been implicated in promoting glioma cell invasion, expansion, and pathogenesis [51–53]. These combined factors formed the rationale for exploiting MMP-14 as a biomarker for imaging glioma. The peptide probes developed here may also be relevant for imaging other malignancies (e.g., breast cancer, melanoma) that overexpress MMP-14 [54–57].

Our imaging approach is unique in that the substrate-binding peptide probe exploits MMP-14 for both enzymatic NIRF signal activation and specific localization of the PET and activated NIRF signals. Most existing PET and activatable fluorescence dual-imaging probes utilize different molecular targets for fluorescence signal activation and binding to the tumor cells. The proposed approach exploits enzymatic amplification of the NIRF signal to enable high-contrast intraoperative imaging of tumors that express activated MMP-14. Exploiting a single biological target for both PET and NIRF reporters can potentially enable straightforward co-registration of the imaging signals for intraoperative fluorescence imaging with high spatial resolution [58–62], which is otherwise challenging when employing separate probes that have differing pharmacokinetic and localization patterns [63]. It remains to be determined if the substrate-binding peptide

first binds to MMP-14, thus preventing the substrate from being activated by the same MMP-14. Mechanistic studies to determine factors affecting peptide cleavage were beyond the scope of our proof-of-concept experiments discussed above. Future experiments will more fully characterize peptide cleavage kinetics and potential mechanisms of inhibition caused by the peptides on MMP-14 enzymatic activity. Since MMP-14 is located on the cell surface, the kinetics in vivo may not be the same as that determined in solution. As endogenous substrates of MMP-14 are large tertiary protein complexes (e.g., proMMP-2, TIMP-2, MMP-14), it is likely a second MMP-14 on the cell surface could process the substrate sequence in the peptide-MMP-14 complex to produce fluorescence activation. Other MMP-14 activatable fluorescence imaging probes do not include a targeted binding moiety, resulting in diffusion of the activated probe away from the target cells [64, 65]. Incorporating the binding peptide into the substrate-binding probe in our studies was anticipated to cause specific retention of the PET and activated NIRF signals on glioma cells, which would enhance signal contrast of the tumor cells relative to adjacent healthy brain. Glioma cell lines showed up to 2.8-fold higher cell-associated NIRF signal at 4 h after in vitro incubation with the substrate-binding peptide relative to the substrate peptide (Fig. 3D; $p < 0.001$), thus supporting the hypothesis that the binding peptide component enhances cell retention of the activated NIRF signal. In addition to ligand-protein interactions that result in signal retention on target cells, factors such as probe extravasation and clearance from tumors also influence TBRs in vivo. The above NIRF imaging results of PDX glioma tumors in resected brain tissues showed comparable TBRs for the substrate-binding peptide and substrate peptide at 4 and 24 h p.i. (Table 1). At the 24 h time point, however, the substrate peptide resulted in the lowest NIRF signal among the groups examined, which is consistent with lower specific retention of the cleaved substrate peptide due to its lack of a binding component.

The results from this work are in agreement with prior studies that have targeted MMP-14 as a biomarker for imaging glioma in preclinical animal models. Favorable PET SUVR (3.9) and NIRF TBR (13.3) signals from the substrate-binding peptide probe were observed in the present studies with an orthotopic PDX glioma model. Previous studies in glioma models or in humans with glioma have used dual-modality imaging probes targeted to other proteins that are overexpressed in glioma relative to normal brain tissue. For instance, preclinical studies using a dual PET/NIRF peptide that binds to EphB4 (Cy5.5-TNYL-RAWK-^{64}Cu-DOTA) in rodents with orthotopic human glioma xenografts indicated TBRs of 9 for PET imaging and 6–7 for fluorescence imaging [58]. A clinical trial using a dual PET/NIRF probe that targets the gastrin releasing peptide receptor (^{68}Ga-BBN-IRDye800) in glioma patients showed a PET SUVR of 13.4 and a NIRF TBR of 4.9 [66].

A primary goal of future studies is to assess if the activatable NIRF probes are suitable for optical-guided resection of glioma models in vivo. The TBRs and specific localization of the NIRF signals in the resected PDX glioma tumors from the present studies suggest the probes would be worthwhile candidates for NIRF-guided resection of glioma. Several preclinical studies in rodents with orthotopic brain tumors have shown TBRs ranging from 3 to 16 for various established (e.g., 5-ALA) or experimental fluorescence imaging agents [14, 32, 33, 63, 67]. Clinical therapy trials in patients with glioma are in progress to evaluate fluorescence-guided resection using imaging agents that include 5-ALA (NCT02119338, NCT01502280, NCT02632370, NCT00752323, NCT02191488, NCT01811121, NCT02379572), ABY-029 (NCT02901925), BLZ-100 (recently completed NCT02234297), panitumumab-IRDye800 (NCT03510208), ^{68}Ga-BBN-IRDye800 (NCT03407781), and fluorescein (NCT03291977, NCT02691923, [68]). These studies highlight the continued thrust to incorporate fluorescence-guided resection to improve outcomes for patients with glioma. Conceptually, it would be ideal to perform fluorescence-guided resection using an imaging probe with minimal photon attenuation in human tissue. While the spectral properties of NIRF fluorophores result in less photon attenuation relative to that of fluorescein or 5-ALA when imaging in human tissues, safe resection is the most critical factor during intraoperative brain tumor surgery. Maintaining the patient's quality of life governs the extent of surgical resection in critical brain tissues, even if those regions contain detectable tumor infiltration, regardless of the sensitivity or specificity of the imaging probe employed during fluorescence-guided resection.

In our pilot studies above, we observed relatively low PET signal in the orthotopic glioma tumors. This result may be due to moderate expression of MMP-14 relative to alternative biomarkers, restricted extravasation of the peptide into tumor parenchyma, moderate molar activity of the radiolabeled probes, sub-optimal mass doses of the probes, or other pharmacokinetic factors. Many small molecule PET probes show moderate accumulation and contrast (TBR 2-5 [69–73]) in glioma, partly due to rapid blood clearance kinetics and short PET radionuclide half-life, while macromolecule-based PET probes often show high accumulation due to significantly longer circulation times that allow the tracer to access tumors through disrupted blood-brain barrier (BBB) regions [13, 74]. The results from the in vivo blocking experiment support the conclusion that the radiolabeled peptide probes showed specific binding in the tumor. It was beyond the scope of these proof-of-concept studies to quantify nonspecific pooling of the probes in glioma tumors due to a disrupted BBB. In human patients, glioma often contains significant portions of tumor cell infiltration in non-contrast-enhancing regions of the brain. Therefore, it would be worthwhile in future experiments to investigate the

accumulation of the novel probes in spontaneous glioma models with tumor invasion in intact BBB regions. The PET studies presented here did not contain an additional method to confirm the size or location of the orthotopic PDX glioma tumors in vivo, although the observed probe uptake in brains during PET imaging was consistent with the histologically confirmed tumor regions identified by H + E and MMP-14 staining of resected brain tissue sections. Due to this limitation, it is possible that the tissue regions selected for in vivo PET measurements could have over- or underestimated the tumor volume and impacted the corresponding SUV results. Having an independent modality, such as MRI, to assess the in vivo tumor volume would increase the rigor of the PET analyses in the orthotopic xenografts. While MMP-14 is expressed in systemic tissues, the presence of tissue inhibitor of MMP-14 (TIMPs) may help minimize its activity in the circulation. Future studies to determine the specificity of glioma-mediated NIRF activation would benefit from comparing NIRF imaging with the probes above to control peptides that either lack the quencher molecule or that have a non-cleavable sequence separating the dye and quencher pair. It would also be useful to determine if different tumor infiltrating cells (e.g., tumor associated glial cells, macrophages) besides glioma cells contribute to the NIRF signal localization from the MMP-14 peptides within the tumor microenvironment [49, 51, 53].

Conclusion

The novel MMP-14 targeted and activatable peptide probes enabled dual PET and NIRF imaging of glioma in preclinical studies. High NIRF signal TBRs were observed in the resected brain sections of mice bearing PDX glioma tumors. Correlations between in vivo PET and ex vivo NIRF signals support the concept for dual-modality imaging of glioma with a single, MMP-14-targeted probe scaffold. The co-localization of NIRF signals and MMP-14 expression in the tumors observed by tissue staining confirmed the specific localization of the peptide probes. These results support future preclinical studies designed to test the efficacy of surgical resection of glioma with the MMP-14-targeted probes.

Materials and methods

General reagents

All general reagents were from commercial suppliers (Thermo Fisher, Waltham, MA, USA; Sigma, St. Louis, MO, USA) unless specified otherwise. Primary antibodies for MMP-14 (rabbit anti-MMP-14 monoclonal antibody (mAb), clone EP1264Y), MMP-2 (rabbit anti-MMP-2 polyclonal, ab37150), or isotype control (rabbit mAb, clone EPR25A) were from Abcam (Cambridge, MA). Fluorophore-conjugated goat anti-rabbit polyclonal secondary antibodies were from Invitrogen (Thermo Fisher). HRP-conjugated secondary antibodies were from Santa Cruz Biotechnology, Inc. (Dallas, TX). The recombinant catalytic enzyme domain of MMP-14 was from Invitrogen. ^{64}Cu was obtained in 0.1 M HCl from the *Mallinckrodt Institute of Radiology PET Nuclear Pharmacy and Cyclotron Facility of the Washington University Medical Center* or from the University of Alabama at Birmingham (UAB) Cyclotron Facility. ^{68}Ga, eluted in 0.1 M HCl from a ^{68}Ge/^{68}Ga generator, was obtained from the UAB Cyclotron Facility.

Gel zymography

Gel zymography was performed as previously described [75]. Briefly, adherent monolayers of glioma cells were rinsed with PBS and incubated in serum-free medium for 24 h. Supernatants were collected, analyzed for protein content, and loaded on zymogram gels (10% gelatin, Novex® Zymogram Gels, Thermo Fisher) according to the manufacturer's recommendations. Relative band intensities were quantified by ImageJ.

Immunofluorescence

Immunocytochemistry: Glioma cells were seeded at 100,000 cells/well in a 12-well plate and allowed to attach overnight. Adherent cells were rinsed in PBS, blocked with 1% BSA in PBS at room temperature for 45 min, incubated with the anti-MMP-14 mAb (Abcam ab51074) or isotype control mAb (Abcam ab172730) at 1 μg/mL in 0.1% BSA in PBS at room temperature for 30 min, rinsed 4 times with 0.1% BSA in PBS, incubated with Ready Probes Alexa Fluor 488-goat anti-rabbit antibody solution (R37116, Molecular Probes, Thermo Fisher) at room temperature for 30 min, rinsed 3 times with 0.1% BSA in PBS, and imaged on an inverted fluorescence microscope at 200× magnification. Mean fluorescence intensity per cell was quantified using ImageJ by randomly selecting 20–25 cells over four fields of view and measuring the mean fluorescence intensity.

Immunohistochemistry: A slide with a formalin-fixed paraffin-embedded (FFPE) human glioma tissue microarray (BS17016b, US Biomax, Inc, Derwood, MD) was deparaffinized and antigen was retrieved by heating for 10 min at 90 °C in citrate buffer pH 6 with 1 mM EDTA. Tissues were blocked in 5% BSA/TBST at room temperature, incubated overnight at 4 °C with anti-MMP-14 mAb at 1 μg/mL in 5% BSA/TBST, washed in TBST, incubated for 2 h at room temperature with Cy5-secondary antibody (A10523, Invitrogen, Thermo Fisher) at 1/1000 dilution in 5% BSA/TBST, rinsed in TBST, and mounted in DAPI-Fluoromount-

G (Southern Biotech, Birmingham, AL). Microarray tissues were imaged on an Odyssey scanner (LI-COR Biosciences, Lincoln, NE) using the 700 nm channel. Integrated instrument software (Image Studio, LI-COR) was used to determine mean fluorescence intensity as total counts/region of interest (ROI) pixel area. 5–6 μm FFPE sections from resected brains of mice bearing orthotopic PDX JX12 glioma tumors were processed using the same protocol, except Alexa Fluor 488-conjugated secondary antibody (A11008, Invitrogen, Thermo Fisher) was used (1/2000 dilution).

Production of peptide probes

The MMP-14 binding, substrate, and substrate-binding peptide probes were synthesized by solid phase techniques using protected amino acids and commercially available IRDye800CW-maleimide and quencher QC-1-NHS ester (LI-COR). The synthesized peptides were purified by semi-preparative reverse-phase high-performance liquid chromatography (RP-HPLC) and characterized by mass spectrometry. Additional details are provided in the Supplementary Materials.

In vitro NIRF activation and NIRF microscopy studies

The catalytic enzyme domain of MMP-14 (5 nM, 5 ng/well) or adherent glioma cells in 96-well plates (Corning Costar, Corning, NY) were incubated with 0.5 μM solutions of the substrate or substrate-binding peptide in 50 μL MMP-14 assay buffer (PBS with 1 mM $CaCl_2$, 0.5 mM $MgCl_2$, 10 μM $ZnCl_2$) at 37 °C, 5% CO_2 for 0–24 h. At designated time points, aliquots (1.5 μL) were removed and spotted on Whatman 1 chromatography paper. After drying at room temperature, NIRF signal of the blots was quantified by the Pearl imaging system (LI-COR). Alternatively, for quantification of the NIRF signal from the substrate peptide, the NIRF signal in the 96-well plates containing glioma cells was directly imaged on the Pearl system. As controls to determine relative fluorescence signal activation at each time point, solutions were used that contained the respective peptide solution without MMP-14 or glioma cells. Cell studies were performed in duplicate wells. For NIRF microscopy studies, glioma cell lines were seeded in 8-chamber slides (10^4 cells/chamber) 2 days before the experiment. On the day of the experiment, cells were rinsed with PBS and incubated at 37 °C, 5% CO_2 with the substrate or substrate-binding peptides (1 μM) in cell medium containing 1% FBS. Chambers were placed on ice at designated time points and medium was aspirated; chambers on ice were washed with ice-cold buffer (PBS, 1% BSA), fixed in formaldehyde at room temperature for 15 min, washed to remove formaldehyde, and mounted in Fluoromount-G prior to NIRF microscopy imaging at 100× magnification. Mean fluorescence intensity per cell was quantified using ImageJ by randomly selecting 30 cells over three fields of view and measuring the mean fluorescence intensity.

In vivo NIRF imaging studies

Mice bearing flank D54 or U87 xenografts (n = 5/group) were injected *i.v.* with 10 nmol substrate peptide or substrate-binding peptide (0.2 mL in PBS). Live, anesthetized mice were imaged on the Pearl system (LI-COR) from 0–24 h *p.i.* Mice bearing orthotopic PDX JX12 xenografts were injected *i.v.* with 0.8–0.9 nmol substrate peptide or substrate-binding peptide (0.2 mL in PBS) and euthanized at 1 h (n = 1 mouse/group), 4 h (n = 4–6 mice/group), or 24 h (n = 3–5 mice/group) *p.i.* Immediately after euthanizing anesthetized mice by cervical dislocation, the skin over the skull was removed, and NIRF signal was determined by the Pearl system. The whole brains were resected, fixed in 10% formalin overnight, and imaged by the Pearl system. Brains were then serially sectioned (1 or 2 mm coronal slices), and all slices were imaged by the Pearl system. Three or four slices containing tumor and adjacent normal brain without tumor were then dehydrated in 70% EtOH and processed for embedding in paraffin and further sectioning (5–6 μm). Unstained sections were imaged on an Odyssey system (LI-COR) or stained for H + E or immunofluorescence (anti-MMP-14 mAb or isotype control) as described above. NIRF signals from the Odyssey scans were defined as positive if they were above the following threshold: three-times the standard deviation above the pooled mean NIRF signal in negative regions (no tumor cells present by H + E histology). Odyssey images and H + E images at the same resolution were compared by ImageJ to define true positive, true negative, false positive, or false negative NIRF signal regions.

In vivo PET/CT imaging studies and biodistribution studies.

Mice bearing orthotopic PDX JX12 xenografts were used for PET/CT imaging and subsequent biodistribution studies with the radiolabeled peptide probes. Mice injected *i.v.* with ^{68}Ga-binding peptide (0.7–1.0 nmol, 2.2–4.5 MBq) with or without unlabeled binding peptide (50 nmol) (n = 3–4 mice/group) were imaged at 1 and 2 h time points *p.i.* Mice injected *i.v.* with ^{64}Cu-substrate-binding peptide (0.3 nmol, 6.3–6.5 MBq) with or without unlabeled binding peptide (22 nmol) (n = 5–6 mice/group) were imaged at 1 and 4 h time points *p.i.* PET (energy window 350–650 KeV; 15 min acquisition for ^{64}Cu studies, 20 min acquisition for ^{68}Ga studies) and CT (voltage 80 kVp, current 150 μA, 720 projections) images were acquired on a GNEXT PET/CT small animal scanner (Sofie Biosciences, Culver City, CA). The PET images were reconstructed using a 3D ordered-subset expectation maximization algorithm (24 subsets and 3 iterations), with random,

attenuation, and decay correction. The CT images were reconstructed using a modified Feldkamp algorithm. Reconstructed images were analyzed using VivoQuant software (version 3.5patch 2, Invicro, LLC, Boston, MA). Following the last imaging time point, anesthetized mice were euthanized by cervical dislocation. Whole brains and other selected tissues were resected, weighed, and counted on a gamma counter (1480 Wizard^2, Perkin Elmer, Shelton, CT). Percent uptake of the injected dose per gram (% ID/g) was calculated by comparing the tissue activity to solutions with known activity of the radionuclide of interest. Resected brains were then fixed in 10% formalin overnight, serially sectioned (1 or 2 mm coronal slices), and processed for further NIRF imaging, paraffin embedding, and tissue sectioning for H + E or immunofluorescence analyses as described above.

Statistical analyses

Data were analyzed using Microsoft Excel or GraphPad Prism (Version 6.1, GraphPad Software, La Jolla, CA, USA). Student's *t*-test was used when comparing two groups. When comparing multiple groups, one-way ANOVA tests, followed by Bonferroni corrections for multiple comparisons, were performed. All *p*-values correspond to two-tailed tests; significance was considered to be at $p < 0.05$.

Acknowledgments Yolanda Hartman, Catherine Langford, Savannah Ferch, Kurt Zinn, Andrew Prince, Marilyn Shackelford, Sally Jordan, Lauren Radford, Charlotte Jeffers, Jennifer Burkemper, Tolulope Aweda, Adriana Massicano, Kiranya Tipirneni, Jonathan McConathy, Suzanne Lapi, Jinda Fan, Jennifer Coleman, Norio Yasui, Dattatray Devalankar, Sharon Samuel, Sheila Bright, Erika McMillian, Himani Modi, Hailey Houson and Morgan Richardson are gratefully acknowledged for their contributions. LI-COR Biosciences is gratefully acknowledged for supplying IRDye800CW-maleimide and QC-1-NHS ester to prepare the peptide probes.

Funding information Funding was provided by the NIH/NINDS T32 UAB Training Program in Brain Tumor Biology (T32 NS048039), the UAB Brain Tumor Core Facility (USPHS NCI P20CA151129), the National Center for Advancing Translational Research of the National Institutes of Health (UL1TR001417), the Department of Defense Congressionally Directed Medical Research Program (CA170769), and the Comprehensive Cancer Center at UAB (NIH P30CA013148).

Compliance with ethical standards

Conflict of interest The authors declare that they have no conflicts of interest.

Ethical approval All applicable international, national, and institutional guidelines for the care and use of animals were followed. Animal studies were approved by the University of Alabama at Birmingham Institutional Animal Care and Use Committee (20366) and performed in compliance with guidelines from the Public Health Service Policy and Animal Welfare Act of the United States. This article does not contain any studies with human participants performed by any of the authors.

Abbreviations *5-ALA*, 5-aminolevulinic acid; *ANOVA*, analysis of variance; BBB, blood-brain barrier; BSA, bovine serum albumin; *CT*, computed tomography; *FDA*, Food and Drug Administration; *FFPE*, formalin-fixed paraffin-embedded; *GBM*, glioblastoma multiforme; *%ID/g*, percent injected dose per g; *i.v.*, intravenous; *mAb*, monoclonal antibody; *MMP*, matrix metalloproteinase; *NIR*, near-infrared; *NIRF*, near-infrared fluorescence; *NOTA*, 1,4,7-triazacyclononane-1,4,7-triacetic acid; *PDX*, patient-derived xenograft; *PET*, positron emission tomography; *p.i.*, post-injection; *PpIX*, protoporphyrin IX; *RIPA*, radioimmunoprecipitation assay; *s.c.*, subcutaneous; *SUVR*, standardized uptake value ratio; *TBR*, tumor-to-background ratio; *UAB*, University of Alabama at Birmingham

References

1. Delgado-López PD, Corrales-García EM. Survival in glioblastoma: a review on the impact of treatment modalities. *Clin Transl Oncol*. **2016**;*18*(11):1062–71.
2. Orringer D, Lau D, Khatri S, Grettel J. Zamora-Berridi; Kathy Zhang; Chris Wu; Neeraj Chaudhary; Oren Sagher, Extent of resection in patients with glioblastoma: limiting factors, perception of resectability, and effect on survival. *J Neurosurg*. **2012**;*117*(5):851–9.
3. Li YM, Suki D, Hess K, Sawaya R. The influence of maximum safe resection of glioblastoma on survival in 1229 patients: can we do better than gross-total resection? *J Neurosurg*. **2016**;*124*(4):977–88.
4. Shiomi T, Okada Y. MT1-MMP and MMP-7 in invasion and metastasis of human cancers. *Cancer Metastasis Rev*. **2003**;*22*(2):145–52.
5. Kessenbrock K, Plaks V, Werb Z. Matrix metalloproteinases: regulators of the tumor microenvironment. *Cell*. **2010**;*141*(1):52–67.
6. Beliën ATJ, Paganetti PA, Schwab ME. Membrane-type 1 matrix metalloprotease (MT1-MMP) enables invasive migration of glioma cells in central nervous system white matter. *J Cell Biol*. **1999**;*144*(2):373–84.
7. Fillmore HL, VanMeter TE, Broaddus WC. Membrane-type matrix metalloproteinases (MT-MMP)s: expression and function during glioma invasion. *J Neuro-Oncol*. **2001**;*53*(2):187–202.
8. Nakada M, Nakamura H, Ikeda E, Fujimoto N, Yamashita J, Sato H, et al. Expression and tissue localization of membrane-type 1, 2, and 3 matrix metalloproteinases in human astrocytic tumors. *Am J Pathol*. **1999**;*154*(2):417–28.
9. Wang L, Yuan J, Tu Y, Mao X, He S, Fu G, et al. Co-expression of MMP-14 and MMP-19 predicts poor survival in human glioma. *Clin Transl Oncol*. **2013**;*15*(2):139–45.
10. Forsyth PA, Wong H, Laing TD, Rewcastle NB, Morris DG, Muzik H, et al. Gelatinase-A (MMP-2), gelatinase-B (MMP-9) and membrane type matrix metalloproteinase-1 (MT1-MMP) are involved in different aspects of the pathophysiology of malignant gliomas. *Br J Cancer*. **1999**;*79*(11-12):1828–35.
11. Yamamoto M, Mohanam S, Sawaya R, Fuller GN, Seiki M, Sato H, et al. Differential expression of membrane-type matrix metalloproteinase and its correlation with gelatinase A activation in human malignant brain tumors *in vivo* and *in vitro*. *Cancer Res*. **1996**;*56*(2):384–92.
12. Gu G, Gao X, Hu Q, Kang T, Liu Z, Jiang M, et al. The influence of the penetrating peptide iRGD on the effect of paclitaxel-loaded MT1-AF7p-conjugated nanoparticles on glioma cells. *Biomaterials*. **2013**;*34*(21):5138–48.
13. de Lucas AG, Schuhmacher AJ, Oteo M, Romero E, Cámara JA, de Martino A, et al. Targeting MT1-MMP as an ImmunoPET-based strategy for imaging gliomas. *PLoS One*. **2016**;*11*(7):e0158634.
14. Shimizu Y, Temma T, Hara I, Makino A, Kondo N, Ozeki E, et al. In vivo imaging of membrane type-1 matrix metalloproteinase with

a novel activatable near-infrared fluorescence probe. *Cancer Sci*. **2014**;*105*(8):1056–62.
15. Albert NL, Weller M, Suchorska B, Galldiks N, Soffietti R, Kim MM, et al. Response assessment in neuro-oncology working group and European Association for Neuro-Oncology recommendations for the clinical use of PET imaging in gliomas. *Neuro-Oncology*. **2016**;*18*(9):1199–208.
16. Kondo A, Ishii H, Aoki S, Suzuki M, Nagasawa H, Kubota K, et al. Phase IIa clinical study of [^{18}F]fluciclovine: efficacy and safety of a new PET tracer for brain tumors. *Ann Nucl Med*. **2016**;*30*(9):608–18.
17. Filss CP, Galldiks N, Stoffels G, Sabel M, Wittsack HJ, Turowski B, et al. Comparison of ^{18}F-FET PET and perfusion-weighted MR imaging: a PET/MR imaging hybrid study in patients with brain tumors. *J Nucl Med*. **2014**;*55*(4):540–5.
18. Piroth MD, Holy R, Pinkawa M, Stoffels G, Kaiser HJ, Galldiks N, et al. Prognostic impact of postoperative, pre-irradiation ^{18}F-fluoroethyl-l-tyrosine uptake in glioblastoma patients treated with radiochemotherapy. *Radiother Oncol*. **2011**;*99*(2):218–24.
19. la Fougère C, Suchorska B, Bartenstein P, Kreth F-W, Tonn J-C. Molecular imaging of gliomas with PET: opportunities and limitations. *Neuro-Oncology*. **2011**;*13*(8):806–19.
20. Tsuyuguchi N, Takami T, Sunada I, Iwai Y, Yamanaka K, Tanaka K, et al. Methionine positron emission tomography for differentiation of recurrent brain tumor and radiation necrosis after stereotactic radiosurgery —In malignant glioma—. *Ann Nucl Med*. **2004**;*18*(4):291–6.
21. Lodge MA, Holdhoff M, Leal JP, Bag AK, Nabors LB, Mintz A, et al. Repeatability of ^{18}F-FLT PET in a multicenter study of patients with high-grade glioma. *J Nucl Med*. **2017**;*58*(3):393–8.
22. Pafundi DH, Laack NN, Youland RS, Parney IF, Lowe VJ, Giannini C, et al. Biopsy validation of ^{18}F-DOPA PET and biodistribution in gliomas for neurosurgical planning and radiotherapy target delineation: results of a prospective pilot study. *Neuro-Oncology*. **2013**;*15*(8):1058–67.
23. Bangiyev L, Rossi Espagnet MC, Young R, Shepherd T, Knopp E, Friedman K, et al. Adult brain tumor imaging: state of the art. *Semin Roentgenol*. **2014**;*49*(1):39–52.
24. Díez Valle R, Tejada Solis S, Idoate Gastearena MA. García de Eulate, R.; Domínguez Echávarri, P.; Aristu Mendiroz, J., Surgery guided by 5-aminolevulinic fluorescence in glioblastoma: volumetric analysis of extent of resection in single-center experience. *J. Neurooncol.* **2011**;*102*(1):105–13.
25. Schucht P, Beck J, Abu-Isa J, Andereggen L, Murek M, Seidel K, et al. Gross total resection rates in contemporary glioblastoma surgery: results of an institutional protocol combining 5-aminolevulinic acid intraoperative fluorescence imaging and brain mapping. *Neurosurgery*. **2012**;*71*(5):927–36.
26. Stummer W, Stocker S, Wagner S, Stepp H, Fritsch C, Goetz C, et al. Intraoperative detection of malignant gliomas by 5-aminolevulinic acid-induced porphyrin fluorescence. *Neurosurgery*. **1998**;*42*(3):518–25 discussion 525-6.
27. Tonn JC, Stummer W. Fluorescence-guided resection of malignant gliomas using 5-aminolevulinic acid: practical use, risks, and pitfalls. *Clin Neurosurg*. **2008**;*55*:20–6.
28. FDA Briefing Information for the May 10, 2017 Meeting of the Medical Imaging Drugs Advisory Committee: NDA 208630 5-ALA (5-aminolevulinic acid HCl). https://www.fda.gov/AdvisoryCommittees/CommitteesMeetingMaterials/Drugs/MedicalImagingDrugsAdvisoryCommittee/ucm557135.htm ().
29. Liu JT, Meza D, Sanai N. Trends in fluorescence image-guided surgery for gliomas. *Neurosurgery*. **2014**;*75*(1):61–71.
30. Belykh E; Martirosyan NL; Yagmurlu K; Miller EJ; Eschbacher JM; Izadyyazdanabadi M; Bardonova LA; Byvaltsev VA; Nakaji P; Preul MC. Intraoperative fluorescence imaging for personalized brain tumor resection: current state and future directions. *Front Surg*. **2016;** *3*:(55).
31. Zhang RR, Schroeder AB, Grudzinski JJ, Rosenthal EL, Warram JM, Pinchuk AN, et al. Beyond the margins: real-time detection of cancer using targeted fluorophores. *Nat Rev Clin Oncol*. **2017**;*14*(6):347–64.
32. Huang R, Vider J, Kovar JL, Olive DM, Mellinghoff IK, Mayer-Kuckuk P, et al. Integrin $\alpha_v\beta_3$-Targeted IRDye 800CW Near-infrared imaging of glioblastoma. *Clin Cancer Res*. **2012**;*18*(20):5731–40.
33. de Souza ALR, Marra K, Gunn J, Samkoe KS, Hoopes PJ, Feldwisch J, et al. Fluorescent affibody molecule administered in vivo at a microdose level labels EGFR expressing glioma tumor regions. *Mol Imaging Biol*. **2017**;*19*(1):41–8.
34. Miller SE, Tummers WS, Teraphongphom N, van den Berg NS, Hasan A, Ertsey RD, et al. First-in-human intraoperative near-infrared fluorescence imaging of glioblastoma using cetuximab-IRDye800. *J Neuro-Oncol*. **2018**;*139*(1):135–43.
35. Cepeda MA, Evered CL, Pelling JJH, Damjanovski S. Inhibition of MT1-MMP proteolytic function and ERK1/2 signalling influences cell migration and invasion through changes in MMP-2 and MMP-9 levels. *J Cell Commun Signal*. **2017**;*11*(2):167–79.
36. Atkinson JM, Falconer RA, Edwards DR, Pennington CJ, Siller CS, Shnyder SD, et al. Development of a novel tumor-targeted vascular disrupting agent activated by membrane-type matrix metalloproteinases. *Cancer Res*. **2010**;*70*(17):6902–12.
37. Ansari C, Tikhomirov GA, Hong SH, Falconer RA, Loadman PM, Gill JH, et al. Development of novel tumor-targeted theranostic nanoparticles activated by membrane-type matrix metalloproteinases for combined cancer magnetic resonance imaging and therapy. *Small*. **2014**;*10*(3):566–75.
38. Mohanty S, Chen Z, Li K, Morais GR, Klockow J, Yerneni K, et al. A novel theranostic strategy for MMP-14-expressing glioblastomas impacts survival. *Mol Cancer Ther*. **2017**;*16*(9):1909–21.
39. Peng X, Chen H, Draney DR, Volcheck W, Schutz-Geschwender A, Olive DM. A nonfluorescent, broad-range quencher dye for Förster resonance energy transfer assays. *Anal Biochem*. **2009**;*388*(2):220–8.
40. Simard B, Tomanek B, van Veggel FC, Abulrob A. Optimal dye-quencher pairs for the design of an "activatable" nanoprobe for optical imaging. *Photochem Photobiol Sci*. **2013**;*12*(10):1824–9.
41. Zhu L, Wang H, Wang L, Wang Y, Jiang K, Li C, et al. High-affinity peptide against MT1-MMP for in vivo tumor imaging. *J Control Release*. **2011**;*150*(3):248–55.
42. Kondo N, Temma T, Shimizu Y, Ono M, Saji H. Radioiodinated peptidic imaging probes for *in vivo* detection of membrane type-1 matrix metalloproteinase in cancers. *Biol Pharm Bull*. **2015**;*38*(9):1375–82.
43. Min K, Ji B, Zhao M, Ji T, Chen B, Fang X, et al. Development of a radiolabeled peptide-based probe targeting MT1-MMP for breast cancer detection. *PLoS One*. **2015**;*10*(10):e0139471.
44. Gill JH, Loadman PM, Shnyder SD, Cooper P, Atkinson JM, Ribeiro Morais G, et al. Tumor-targeted prodrug ICT2588 demonstrates therapeutic activity against solid tumors and reduced potential for cardiovascular toxicity. *Mol Pharm*. **2014**;*11*(4):1294–300.
45. Snyman C, Niesler CU. MMP-14 in skeletal muscle repair. *J Muscle Res Cell Motil*. **2015**;*36*(3):215–25.
46. Giannini C, Sarkaria JN, Saito A, Uhm JH, Galanis E, Carlson BL, et al. Patient tumor EGFR and PDGFRA gene amplifications retained in an invasive intracranial xenograft model of glioblastoma multiforme. *Neuro-Oncology*. **2005**;*7*(2):164–76.
47. Oliva CR, Nozell SE, Diers A, McClugage SG 3rd, Sarkaria JN, Markert JM, et al. Acquisition of temozolomide chemoresistance in gliomas leads to remodeling of mitochondrial electron transport chain. *J Biol Chem*. **2010**;*285*(51):39759–67.

48. Bourboulia D, Stetler-Stevenson WG. Matrix metalloproteinases (MMPs) and tissue inhibitors of metalloproteinases (TIMPs): positive and negative regulators in tumor cell adhesion. *Semin Cancer Biol*. **2010**;*20*(3):161–8.
49. Ulasov I, Yi R, Guo D, Sarvaiya P, Cobbs C. The emerging role of MMP14 in brain tumorigenesis and future therapeutics. *Biochimi Biophysic Acta*. **2014**;*1846*(1):113–20.
50. Devy L, Huang L, Naa L, Yanamandra N, Pieters H, Frans N, et al. Selective inhibition of matrix metalloproteinase-14 blocks tumor growth, invasion, and angiogenesis. *Cancer Res*. **2009**;*69*(4):1517–26.
51. Markovic DS, Vinnakota K, Chirasani S, Synowitz M, Raguet H, Stock K, et al. Gliomas induce and exploit microglial MT1-MMP expression for tumor expansion. *Proc Natl Acad Sci U S A*. **2009**;*106*(30):12530–5.
52. Markovic DS, Vinnakota K, van Rooijen N, Kiwit J, Synowitz M, Glass R, et al. Minocycline reduces glioma expansion and invasion by attenuating microglial MT1-MMP expression. *Brain Behav Immun*. **2011**;*25*(4):624–8.
53. Charles NA, Holland EC, Gilbertson R, Glass R, Kettenmann H. The brain tumor microenvironment. *Glia*. **2011**;*59*(8):1169–80.
54. McGowan PM, Duffy MJ. Matrix metalloproteinase expression and outcome in patients with breast cancer: analysis of a published database. *Ann Oncol*. **2008**;*19*(9):1566–72.
55. Määttä M, Soini Y, Liakka A, Autio-Harmainen H. Differential expression of matrix metalloproteinase (MMP)-2, MMP-9, and membrane type 1-MMP in hepatocellular and pancreatic adenocarcinoma: implications for tumor progression and clinical prognosis. *Clin Cancer Res*. **2000**;*6*(7):2726–34.
56. Hofmann UB, Westphal JR, Zendman AJ, Becker JC, Ruiter DJ, van Muijen GN. Expression and activation of matrix metalloproteinase-2 (MMP-2) and its co-localization with membrane-type 1 matrix metalloproteinase (MT1-MMP) correlate with melanoma progression. *J Pathol*. **2000**;*191*(3):245–56.
57. Imanishi Y, Fujii M, Tokumaru Y, Tomita T, Kanke M, Kanzaki J, et al. Clinical significance of expression of membrane type 1 matrix metalloproteinase and matrix metalloproteinase-2 in human head and neck squamous cell carcinoma. *Hum Pathol*. **2000**;*31*(8):895–904.
58. Huang M, Xiong C, Lu W, Zhang R, Zhou M, Huang Q, et al. Dual-modality micro-positron emission tomography/computed tomography and near-infrared fluorescence imaging of EphB4 in orthotopic glioblastoma xenograft models. *Mol Imaging Biol*. **2014**;*16*(1):74–84.
59. Li C, Wang W, Wu Q, Ke S, Houston J, Sevick-Muraca E, et al. Dual optical and nuclear imaging in human melanoma xenografts using a single targeted imaging probe. *Nucl Med Biol*. **2006**;*33*(3):349–58.
60. Sampath L, Kwon S, Ke S, Wang W, Schiff R, Mawad ME, et al. Dual-labeled trastuzumab-based imaging agent for the detection of human epidermal growth factor receptor 2 overexpression in breast cancer. *J Nucl Med*. **2007**;*48*(9):1501–10.
61. Kimura RH, Miao Z, Cheng Z, Gambhir SS, Cochran JR. A dual-labeled knottin peptide for PET and near-infrared fluorescence imaging of integrin expression in living subjects. *Bioconjug Chem*. **2010**;*21*(3):436–44.
62. Olson ES, Jiang T, Aguilera TA, Nguyen QT, Ellies LG, Scadeng M, et al. Activatable cell penetrating peptides linked to nanoparticles as dual probes for in vivo fluorescence and MR imaging of proteases. *Proc Natl Acad Sci U S A*. **2010**;*107*(9):4311–6.
63. Elliott JT, Marra K, Evans LT, Davis SC, Samkoe KS, Feldwisch J, et al. Simultaneous *in vivo* fluorescent markers for perfusion, protoporphyrin metabolism, and EGFR expression for optically guided identification of orthotopic glioma. *Clin Cancer Res*. **2017**;*23*(9):2203–12.
64. Zhu L, Zhang F, Ma Y, Liu G, Kim K, Fang X, et al. In vivo optical imaging of membrane-type matrix metalloproteinase (MT-MMP) activity. *Mol Pharm*. **2011**;*8*(6):2331–8.
65. Gao S, Zhang L, Wang G, Yang K, Chen M, Tian R, et al. Hybrid graphene/Au activatable theranostic agent for multimodalities imaging guided enhanced photothermal therapy. *Biomaterials*. **2016**;*79*:36–45.
66. Li D, Zhang J, Chi C, Xiao X, Wang J, Lang L, et al. First-in-human study of PET and optical dual-modality image-guided surgery in glioblastoma using ^{68}Ga-IRDye800CW-BBN. *Theranostics*. **2018**;*8*(9):2508–20.
67. Ribeiro de Souza AL, Marra K, Gunn J, Samkoe KS, Hull S, Paulsen KD, et al. Optimizing glioma detection using an EGFR-targeted fluorescent affibody. *Photochem Photobiol*. **2018**;*94*(6):1167–71.
68. Acerbi F, Broggi M, Schebesch K-M, Höhne J, Cavallo C, De Laurentis C, et al. Fluorescein-guided surgery for resection of high-grade gliomas: a multicentric prospective phase II study (FLUOGLIO). *Clin Cancer Res*. **2018**;*24*(1):52–61.
69. Suchorska B, Jansen NL, Linn J, Kretzschmar H, Janssen H, Eigenbrod S, et al. Biological tumor volume in ^{18}FET-PET before radiochemotherapy correlates with survival in GBM. *Neurology*. **2015**;*84*(7):710–9.
70. Verger A, Filss CP, Lohmann P, Stoffels G, Sabel M, Wittsack HJ, et al. Comparison of ^{18}F-FET PET and perfusion-weighted MRI for glioma grading: a hybrid PET/MR study. *Eur J Nucl Med Mol Imaging*. **2017**;*44*(13):2257–65.
71. Dunet V, Pomoni A, Hottinger A, Nicod-Lalonde M, Prior JO. Performance of ^{18}F-FET versus ^{18}F-FDG-PET for the diagnosis and grading of brain tumors: systematic review and meta-analysis. *Neuro-Oncology*. **2016**;*18*(3):426–34.
72. Yoo MY, Paeng JC, Cheon GJ, Lee DS, Chung JK, Kim EE, et al. Prognostic value of metabolic tumor volume on ^{11}C-methionine PET in predicting progression-free survival in high-grade glioma. *Nucl Med Mol Imaging*. **2015**;*49*(4):291–7.
73. Doi Y, Kanagawa M, Maya Y, Tanaka A, Oka S, Nakata N, et al. Evaluation of trans-1-amino-3-^{18}F-fluorocyclobutanecarboxylic acid accumulation in low-grade glioma in chemically induced rat models: PET and autoradiography compared with morphological images and histopathological findings. *Nucl Med Biol*. **2015**;*42*(8):664–72.
74. Yang Y, Hernandez R, Rao J, Yin L, Qu Y, Wu J, et al. Targeting CD146 with a ^{64}Cu-labeled antibody enables in vivo immunoPET imaging of high-grade gliomas. *Proc Natl Acad Sci U S A*. **2015**;*112*(47):E6525–34.
75. Merrell MA, Ilvesaro JM, Lehtonen N, Sorsa T, Gehrs B, Rosenthal E, et al. Toll-like receptor 9 agonists promote cellular invasion by increasing matrix metalloproteinase activity. *Mol Cancer Res*. **2006**;*4*(7):437–47.